Supporting Information

EMM-17 as an efficient catalyst for the one-step conversion of high-concentration lactic acid into lactide

Binyao Feng, [†a] Kunhao Shen, [†a] Chenxu Liu, [ab] Xingrui Wang, [c] Cailing Chen, [b] Jian Zhang, [d] Huiyong Chen, [c] Feijian Chen, [*ab] Yi Li, [*ab] Jihong Yu [*ab]

[a] State Key Laboratory of Inorganic Synthesis and Preparative Chemistry, College of Chemistry, Jilin University, Changchun 130012, P. R. China

[b] International Center of Future Science, Jilin University, Changchun 130012, P. R. China

[c] School of Chemical Engineering, Northwest University, Xi'an, Shaanxi 710069, P. R. China

[d] Beijing Advanced Innovation Center for Soft Matter, Science and Engineering, Beijing University of Chemical Technology, Beijing, P. R. China

† These authors contributed equally to this work.

Contents

1 Experimental Sections and Characterizations

1.1 Chemicals and reagents

All chemicals and reagents were supplied by commercial suppliers and used without further purification: Tetraethylorthosilicate (TEOS, Macklin Company), 4-(pyrrolidine-1-yl) pyridine (97%, Innochem chemical), Iodoethane (99.9%, Innochem chemical), Aluminum nitrate nonahydrate ($Al(NO_3)_3$, 99.0%, Innochem chemical), Hydrofluoric acid (HF, 40%, Aladdin chemical), Amberlite IRN-78 (ion exchange resin, nuclear grade Alfa Aesar Company), H-Beta zeolite (Si/Al = 12.5, Alfa Aesar Company), Tetrapropylammonium hydroxide solution (TBAOH, 25wt%, Sinopharm Chemical Reagent Co, Ltd.), Tetrapropylammonium hydroxide solution (TPAOH, 25wt%, Sinopharm Chemical Reagent Co, Ltd.), Aluminium isopropoxide (99.99%, Innochem chemical), Ammonium fluoride (99.99%, Innochem chemical), Sodium aluminate ($NaAlO_2$, CP, Sinopharm Chemical Reagent Co, Ltd.), L-Lysine (98%, Innochem chemical), Sodium hydroxide (NaOH, AR, 98%, Tianjin Yongsheng Chemical Reagent Co, Ltd.), Ammonium nitrate (95%, Supelco), Lactic acid (LA, 105 wt%, Zhejiang Hisun Biomaterials Company), Toluene (99.5%, Tianjin Xintong Chemical Reagent Co, Ltd.).

1.2 Synthesis

Synthesis of ODSA, 1-ethyl-4-(pyrrolidin-1-yl) pyridine-1-ium hydroxide

Iodoethane (19.5g) was added to a solution of 4-(pyrrolidine-1-yl) pyridine (14.821g) dissolved in ethanol (80ml). The reaction was heat at 60 °C and stirred for 1 days. The ethanol solvent and excess iodoethane were removed by rotary evaporation, yielding a colorless oily liquid. Subsequently, tetrahydrofuran (THF) was slowly added to the reaction flask under stirring and heating at 80 ℃. The formation of fine white particulate solids was observed. The solids were collected by filtration, washed with THF, and dried to afford the product as the iodide salt. The iodide salt was subsequently converted to a hydroxide solution by column ion-exchange using an excess of anion exchange resin.

Synthesis of EMM-17 zeolite

In a typical process, a specified mass of OSDA solution was charged into the reaction vessel. Under stirring, a specified volume of aluminum nitrate solution was added, followed by the addition of 0.45 mL tetraethyl orthosilicate (TEOS). After hydrolysis for 5 hours, 0.256 mL of 40% hydrofluoric acid (HF) solution was introduced. Stirring was continued for an additional 30 minutes. The stir bar was then removed, and the mixture was transferred to an 80 ℃ oven to evaporate excess water until the theoretical weight was attained. The gel composition was SiO_2: 0.8 OSDAOH: 0.0167 Al_2O_3: 0.8 HF: 5 H_2O. The resulting solid was transferred into a 3 mL Teflon-lined stainless-steel autoclave and subjected to crystallization at 160 ℃ for 5 days. The as-prepared solid samples were centrifuged, washed with water and ethanol several times, and dried at 80 ℃ in the oven overnight. And then calcined at 550 ℃ for 6 h to remove template.

Synthesis of ZSM-5 zeolite.

Initially, 7.33 g of a 40 wt.% aqueous solution of tetrapropylammonium hydroxide (TPAOH) was mixed with 5 ml of deionized water. Subsequently, 4.23 g of tetraethyl orthosilicate (TEOS) was added, and the mixture was stirred to allow for hydrolysis. Following hydrolysis, 0.058 g of sodium aluminate was introduced, and finally, 1.12 g of L-lysine was added. The resulting mixture was stirred thoroughly and then transferred into the Teflon liner of a stainless-steel autoclave. First-stage crystallization was performed at 90 ℃ for 2 days, followed by second-stage crystallization at 170 ℃ for 1 day. The as-prepared solid samples were centrifuged, washed with water and ethanol several times, and dried at 80 ℃ in the oven overnight. And then calcined at 550 ℃ for 6 h to remove template.

Synthesis of ZSM-5-M zeolite.

1 g of the aforementioned synthesized ZSM-5 zeolite was treated with 20 g of a 40wt% aqueous ammonium fluoride (NH_4F) solution at 50 ℃ for 5 minutes under stirring. The solid product was then recovered by centrifugation, rinsed repeatedly with deionized water until the supernatant reached a neutral pH, and dried. The resulting material,

denoted as ZSM-5-M, was obtained via the etching method. And then calcined at 550 ℃ for 6 h to remove template.

Synthesis of self-pillared pentasil (SPP) zeolite

Initially, 12.4 g of a 40 wt.% aqueous tetrabutylammonium hydroxide (TBAOH) solution was thoroughly mixed with 3.0 g of deionized water. Subsequently, 122 mg of aluminum isopropoxide was added, and the mixture was stirred for 30 minutes. Following this, 12 mg of sodium hydroxide (NaOH) and 12.48 g of tetraethyl orthosilicate (TEOS) were introduced. Stirring was continued for 4 hours to ensure complete hydrolysis of TEOS. The resulting homogeneous solution was transferred into a 100 mL Teflon-lined stainless-steel autoclave. Hydrothermal crystallization was performed in an oven using a two-stage temperature profile: first at 80 ℃ for 1 day (low-temperature pre-crystallization), followed by further crystallization at 160 ℃ for 2 days. The synthesized solid product was recovered by centrifugation and sequentially washed with deionized water and absolute ethanol until neutral. The purified material was dried at 80 ℃ for 12 hours. To remove organic templates, calcination was conducted at 550 ℃ for 6 hours under static air. The calcined zeolite was converted to its protonated form via ion exchange. This involved three cycles of treatment with an aqueous ammonium nitrate solution (1 M) under stirring at 80 ℃ for 4 hours, with intermediate centrifugation and washing steps. The final H-SPP product was dried overnight at 80 ℃. And then calcined at 550 ℃ for 6 h to remove template.

1.3 Characterizations

Scanning electron microscopy images were measured with JEOL JSM-7800F. The transmission electron microscopy images were measured with Tencai F20 and Thermo Fisher Scientific (FEI) Talos F200s electron microscope. iDPC-STEM experiments were performed using a double Cs-corrected microscope (FEI Titan Cubed Themis Z), operated at 300 kV. The powder X-ray diffraction measurements were performed on a Rigaku Miniflex 300 diffractometer by using Cu Kα radiation. Nitrogen adsorption/desorption isotherms were measured on BSD-660 high performance physical adsorption analyzer at 77 K. The materials (100 mg) were degassed under

vacuum at 350 ℃ for 12 h before nitrogen adsorption at −196 ℃. The solid-state nuclear resonance (NMR) spectra of ^{27}Al and ^{29}Si were collected using the magic-angle spinning (MAS) technique on a JEOL ECZ500R NMR spectromenter, operating at the frequencies of 79.49 and 100.62 MHz, respectively. NH_3-TPD was performed on Micromeritics/Autochem II 2920, from 100 to 550 ℃ (ramp rate 10 ℃ min^{-1}) under He (60 cm^3 min^{-1}), with desorbed NH_3 monitored by thermal conductivity. Thermogravimetric (TG) analysis was performed on a TA company TGA Q500 unit at a heating rate of 10 ℃ min^{-1} from room temperature to 800 ℃ in air. The Py-FTIR test was carried out using Bruker EQUINOX55 infrared spectrometer. *In situ* FT-IR spectra of 2,4,6-tri-tert-butylpyridine (TTBP) adsorption were measured on a Bruker VERTEX 70 infrared spectrometer equipped with an in situ cell. [1] [2]

1.4 Silylation treatment

For the TBCS-silylation treatment, the entire process was carried out in a fixed-bed reactor. First, EMM-17 was filled into a quartz reactor tube. One end of the tube was connected to an injection needle containing TBCS, and TBCS was transported to the quartz tube by pulsed injection using N_2 as the carrier gas. Another end of the quartz tube was connected to a diaphragm vacuum pump to remove the TBCS physically absorbed by EMM-17. The specific silylation process was carried out according to the following steps: First, 1.0 g of EMM-17 sample (40-60 mesh) was weighed, and the EMM-17 was pre-treated at 500 ℃ under N_2 gas for 2 hours. Then, the reaction furnace temperature was adjusted to the temperature required for silylation (usually 450 ℃). Next, TBCS carried by N_2 (30 mL/min) was vaporized and reacted with EMM-17 for 4 hours. Subsequently, the sample was purged with N_2 (30 mL/min) for 2 hours, and then maintained at the same temperature, and in situ degassing treatment was carried out using a static vacuum system for 12 hours to remove the physically adsorbed TBCS. Finally, the sample was calcined at 550 ℃ in an air atmosphere for 6 hours to remove the carbon-hydrocarbon organic groups.

1.5 Density Functional theory calculation

In this work, the DFT calculations have been conducted using the Vienna Ab initio Simulation Package (VASP), [3] which operates on a plane wave basis. The projective augmented wave (PAW) method is employed to model the interaction between electrons and ions, [4, 5] while the generalized gradient approximation (GGA) with the Perdew-Burke-Ernzerhof (PBE) functional is applied to address exchange interactions and related effects. [6] A plane-wave cutoff energy of 450 eV is utilized, with k-point sampling restricted to the Gamma point. Convergence during the iterative process was reached when the force and energy differences are less than 0.05 eV/Å and 10^{-5} eV, respectively. Transition states were identified using the CI-NEB and Dimer methods. [7, 8] Additionally, vibrational frequency analysis was carried out to distinguish between minimum and transition states, as well as to calculate free energy.

In this work, the initial bulk zeolite structures of EMM-17A and EMM-17B were selected from International Zeolite Association structure database. Based on the TEM results, EMM-17 is identified as a layered material with the [010] crystal plane exhibiting the largest exposed area. According to the surface energy calculation formula, a lower number of surface hydroxyl groups corresponds to lower energy and greater structural stability. Therefore, the half-ring surface configuration cut from the [010] crystal plane is utilized for subsequent calculations. To minimize periodic boundary effects in the direction normal to the surface, a vacuum layer of 20 Å was added along the c-axis to create the EMM-17 [010] model. The lattice parameters measured of optimized EMM-17 was 12.5955×24.7418×34.9426 $Å^3$ and angles $a=\beta=\gamma=90°$.

2 Catalytic tests

Typically,1.0 g of EMM-17 zeolite catalyst, 1.0 g 105 wt.% LA feedstock, and 20mL of toluene were added in a 25mL round bottom flask under magnetic stirring. On top of the setup, a phase-settler/solvent reflux trap was installed, filled beforehand with 25 mL of toluene. This setup assured reflux of toluene while trapping water. The solvent floated on top and moved to the flask while the water sinked to the bottom of the trap where it accumulated. The oil bath was held at 140 ℃ to assure reflux. Under

continuous stirring, 0.4 mL of the mixture was taken out at different time intervals during 5 h. Then the withdrawn mixture was added with excess acetonitrile, and placed for three hours. Three hour later, the mixture was filtered with Syringe Filter (PTFE, 0.2 μm) to isolate the solid zeolites. The filtered solution was divided and dried under vacuum at room temperature for 24 h to remove toluene and acetonitrile solvents for HPLC and ^{1}H-NMR analysis based on the work by Dusselier *et al*. [9]

High pressure liquid chromatography (HPLC) and proton nuclear magnetic resonance spectroscopy (^{1}H-NMR) was adopted for determining product yields and LA conversion.

HPLC: The dried sample was dissolved in water: acetonitrile mixture (50: 50, V: V), then the solution with 2 mg/mL was qualitatively analyzes by HPLC. This method was based on the work by Dusselier *et al*. HPLC measurements were conducted with an Agilent 1200 series HPLC system (pump, UV/Visible (UV/Vis) Detector at 210nm). The flow rate was 1.0 mL/min on a C_{18} column oven temperature was maintained at 25 ℃. Two solvents were used in the elution program: a) water (with addition of 2mL of 85% H_3PO_4 per Liter); b) 100% acetonitrile (with addition of 2mL of 85% H_3PO_4 per Liter). The elution program (a/b, V/V) was as follows: minute 0-1: 90/10; minute 1-3: linear ramp to 10/90; minute 3-10: 10/90; and minute 10-20: return to 90/10. From HPLC spectra, the proportion of LA, L_2A, L_3A, L_nA (n >3) and LT were estimated according to formula below:

LA proportion (%) = [(LA area% of the sample) / (all area%)] *100%

L_2A proportion (%) = [(L_2A area% of the sample) / (all area%)] *100%

L_3A proportion (%) = [(L_3A area% of the sample) / (all area%)] *100%

L_nA proportion (%) = [(L_nA area% of the sample) / (all area%)] *100%

LT proportion (%) = [(LT area% of the sample) / (all area%)] *100%

^{1}H-NMR: The chemical structures of the reaction mixtures were calculated based on ^{1}H-NMR (Bruker Avance 300) and d6-dimethyl sulfoxide (d6-DMSO) was used as the solvent. As shown in Figures S13, signals from 5.5 ppm (A) were assigned to the

methine proton of the lactide, while the methine proton signals corresponding to the oligomers segment appeared at 5.2 ppm (C), 5.0 ppm (B), 4.2 ppm (D) were derived from carboxylic end groups of oligomers, centers of oligomers, and hydroxyl end groups of oligomers, respectively. The methine proton signals derived from the lactic acid were detected at 4.0 ppm (E). From ^{1}H-NMR spectra, the lactide yield was estimated according to formula: LT5 yield (mol%) = (A / A+B+C+D+E)×100.

The lactide yields form these two characterization techniques were in good agreement (< 5% difference).

3 Supplementary Figures and Tables

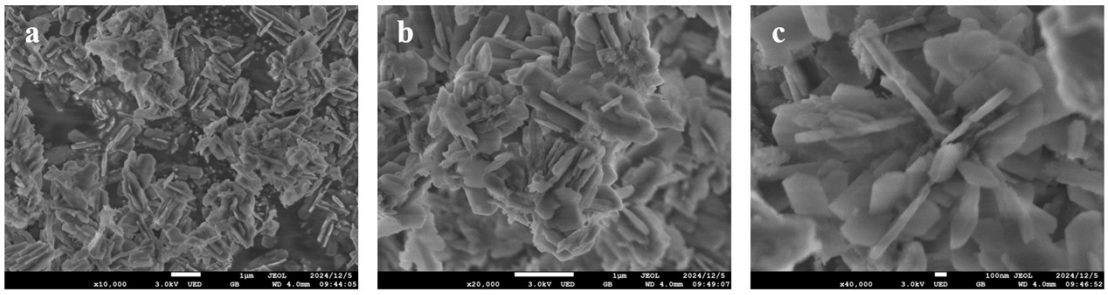

Fig.S1 SEM images of as-made EMM-17

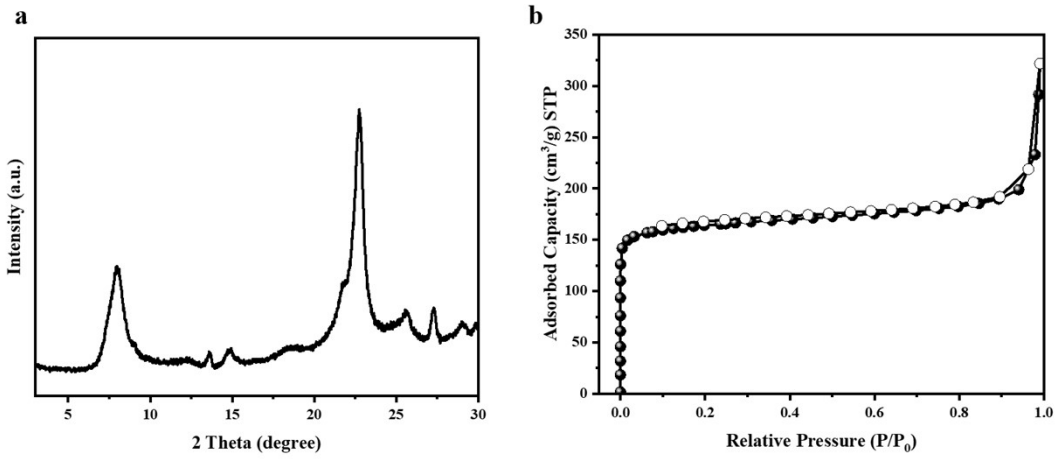

212

213 Fig.S2 (a) PXRD patterns and (b) N_2 adsorption-desorption isotherms of Beta-C

214

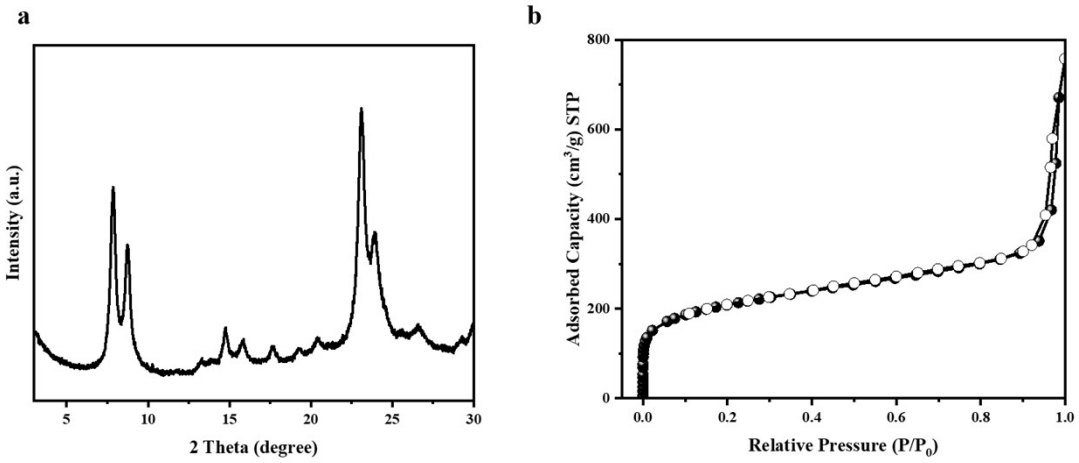

215

216 Fig.S3 (a) PXRD patterns and (b) N_2 adsorption-desorption isotherms of SPP

217

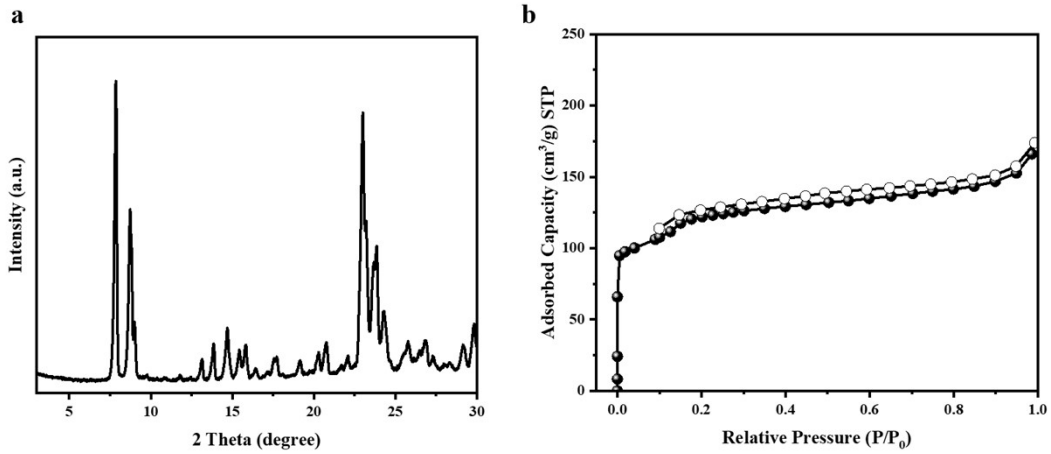

218

219 Fig.S4 (a) PXRD patterns and (b) N_2 adsorption-desorption isotherms of ZSM-5

220

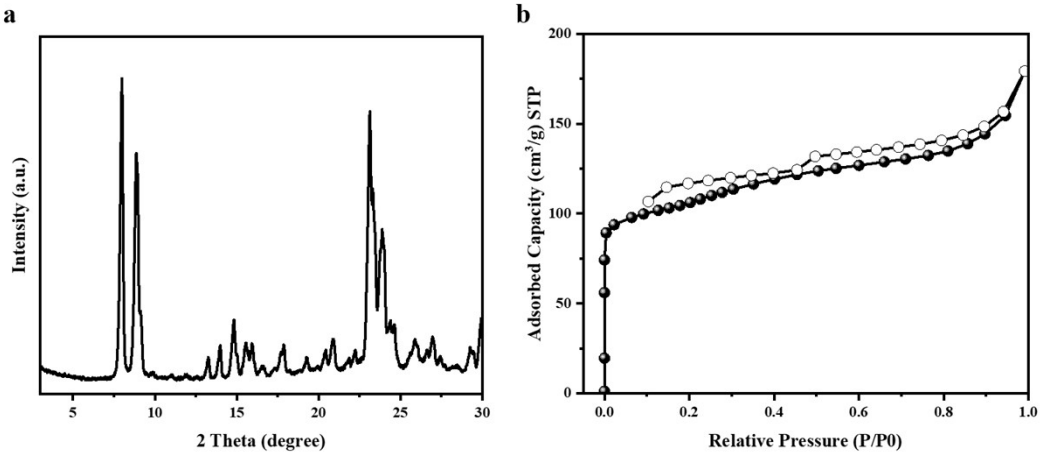

221

222 Fig.S5 (a) PXRD patterns and (b) N_2 adsorption-desorption isotherms of ZSM-5-M

223

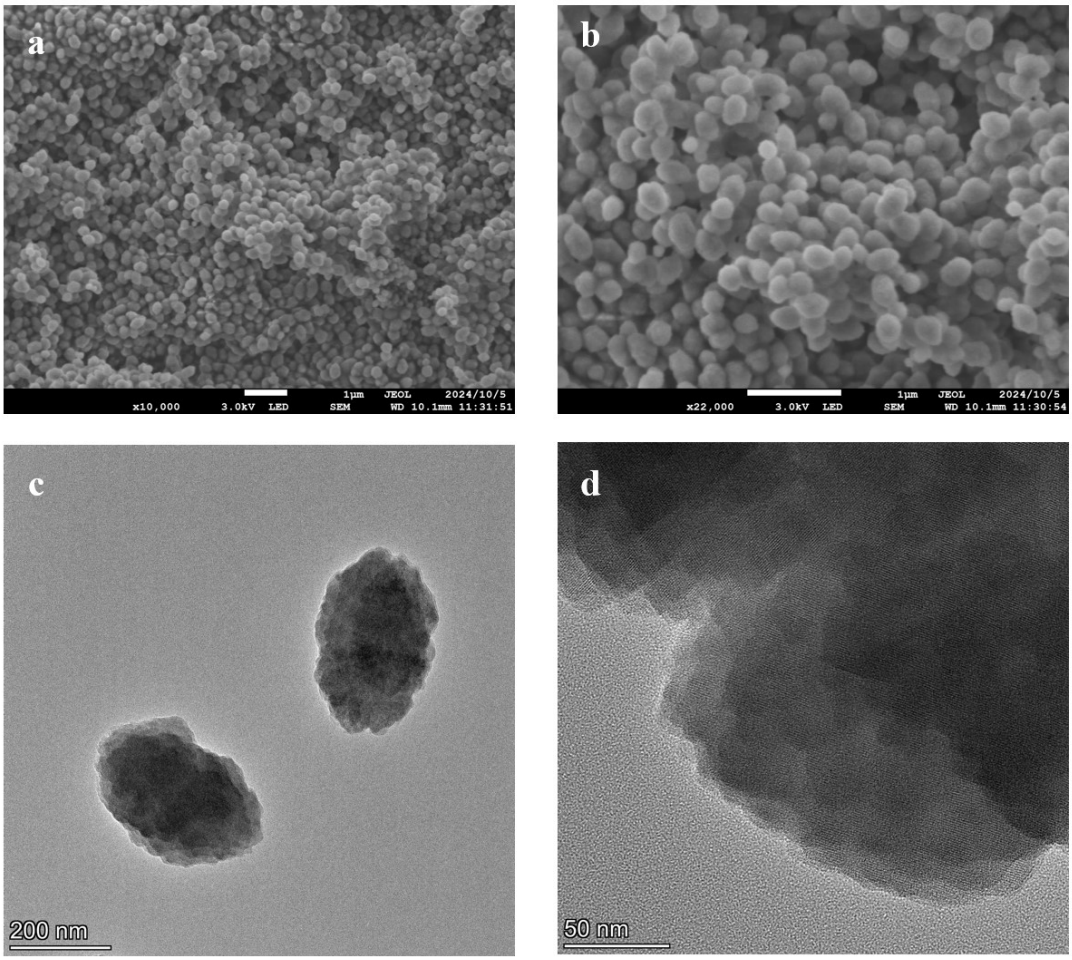

Fig.S6 (a, b) SEM images and (c, d) TEM images of Beta-C

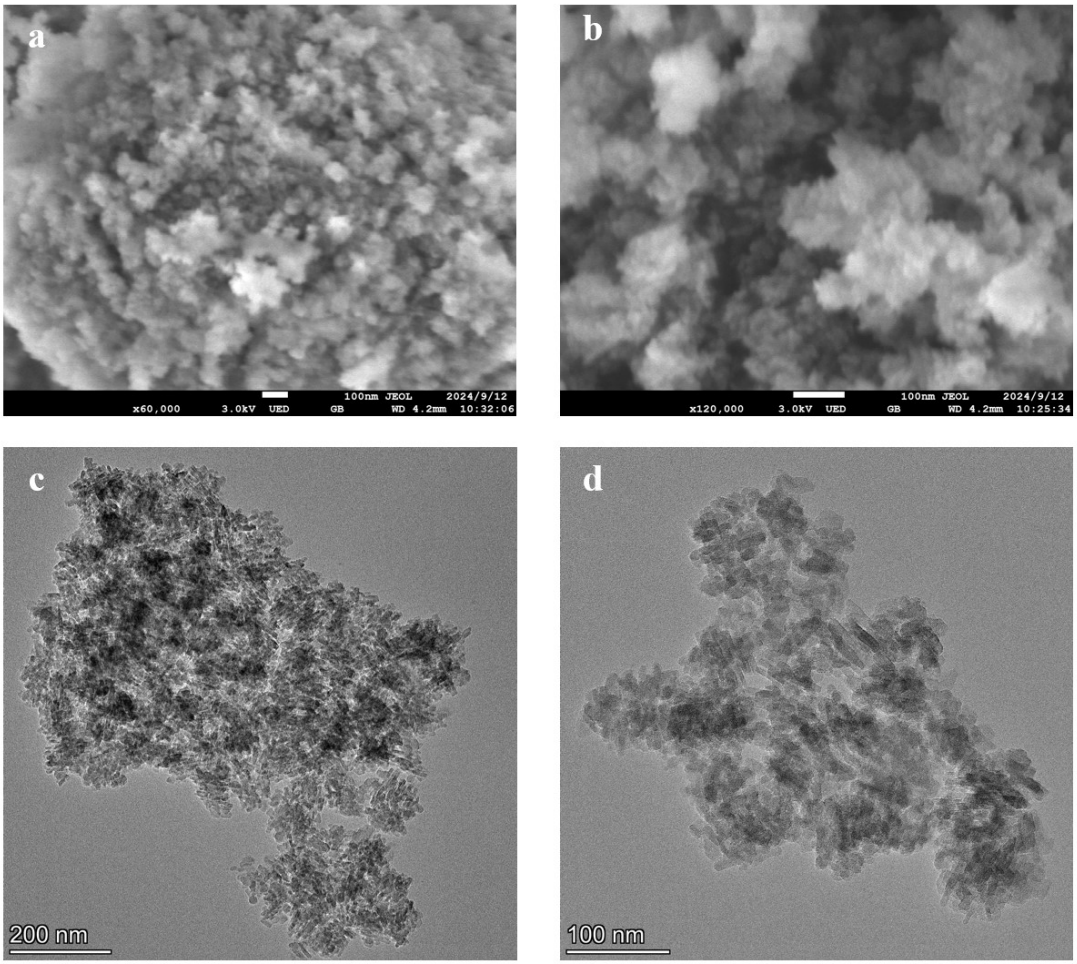

Fig.S7 (a, b) SEM images and (c, d) TEM images of SPP

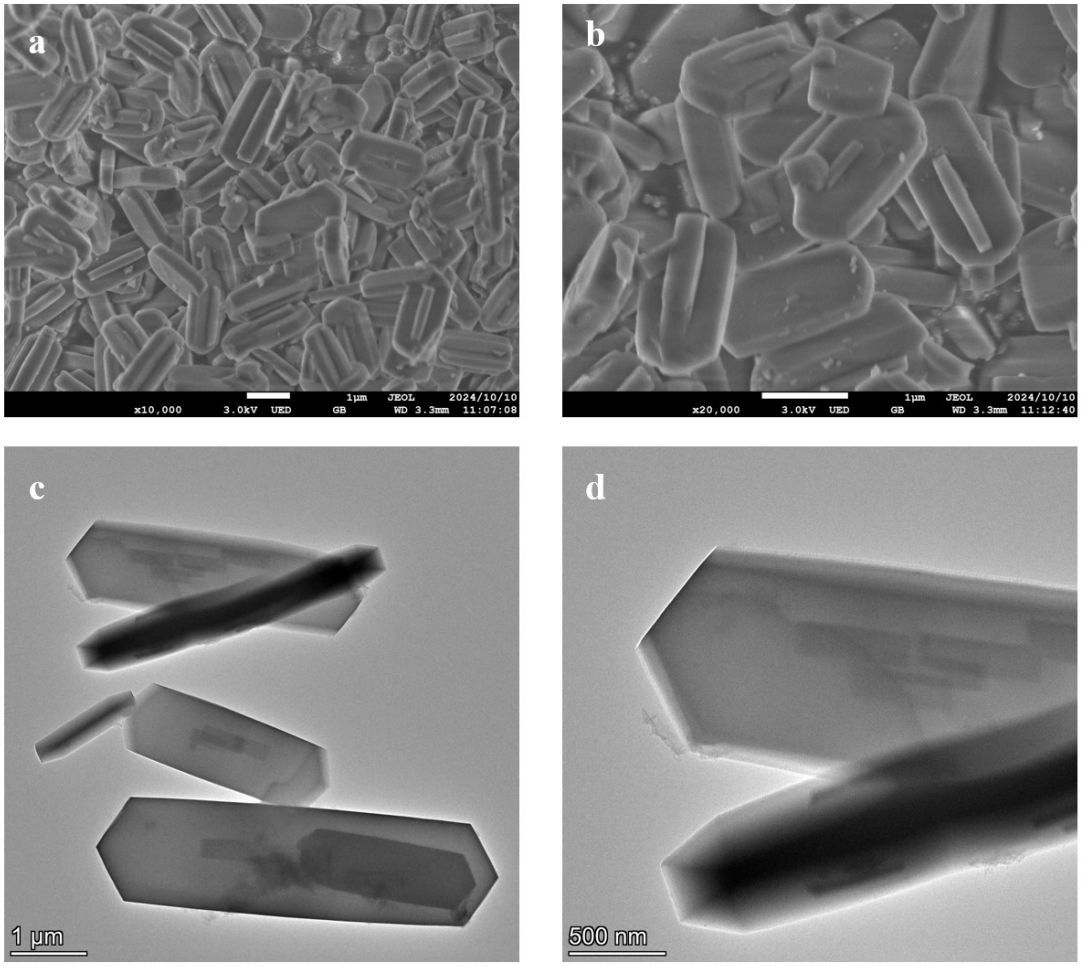

228

229 Fig.S8 (a, b) SEM images and (c, d) TEM images of ZSM-5

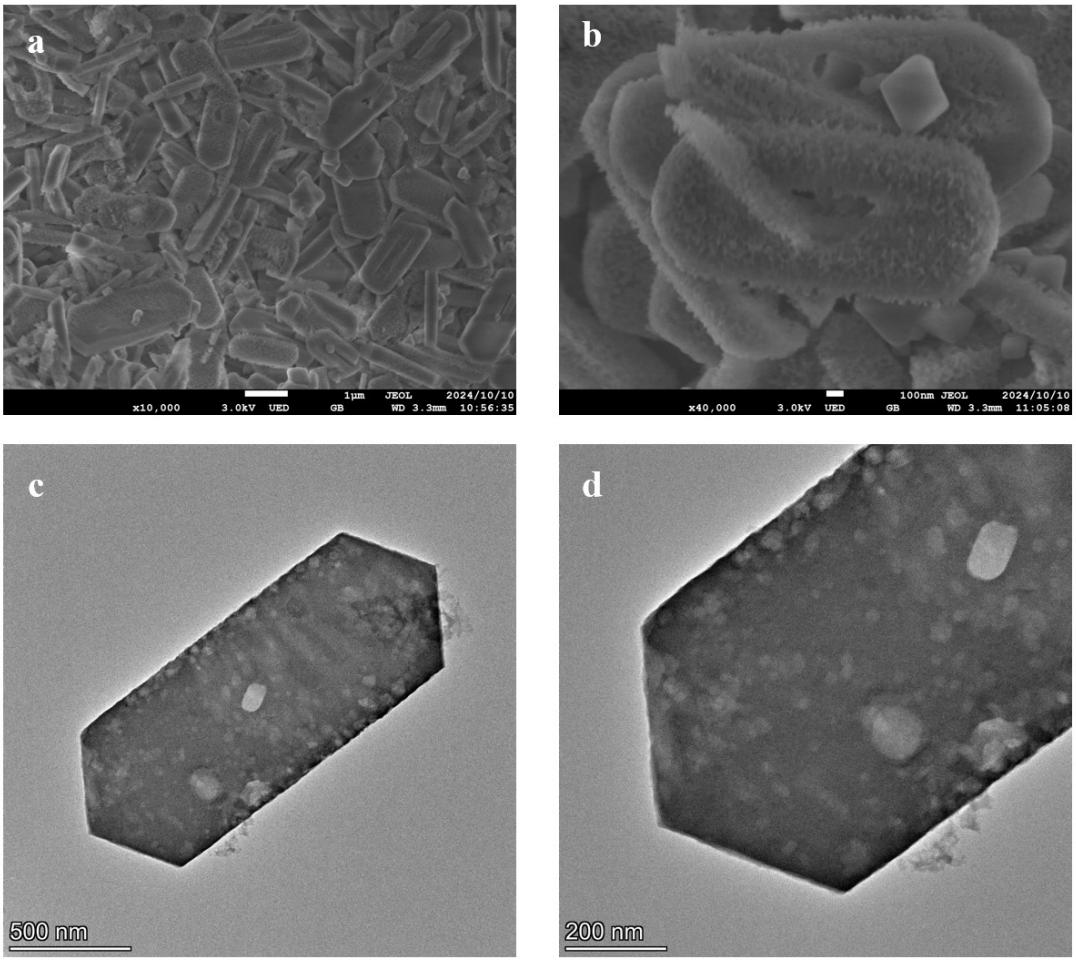

Fig.S9 (a, b) SEM images and (c, d) TEM images of ZSM-5-M

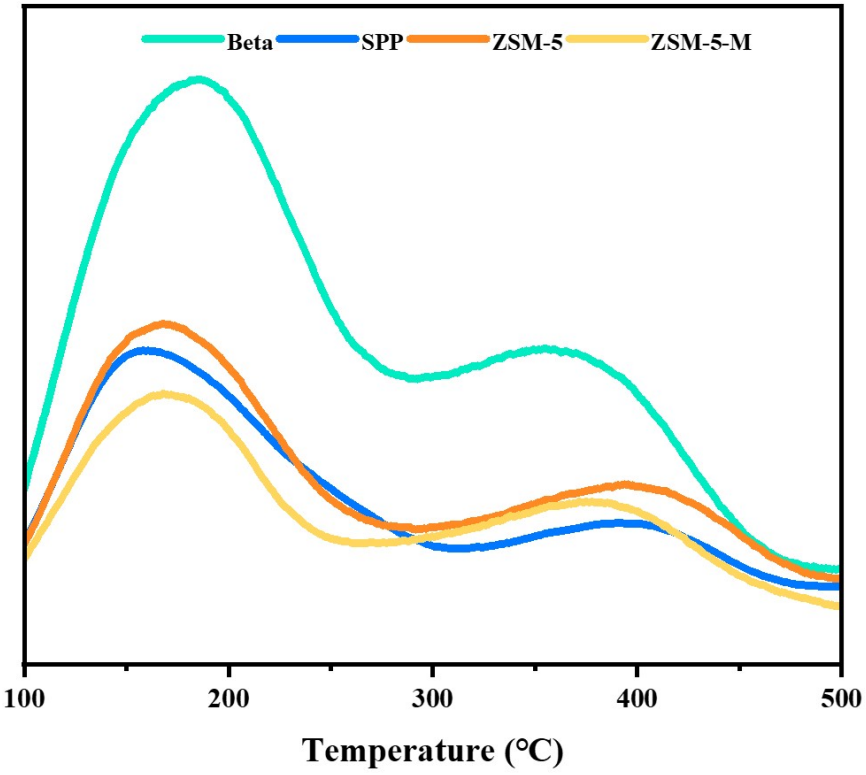

232

233 Fig.S10 NH_3-TPD profiles of comparison catalysts

234

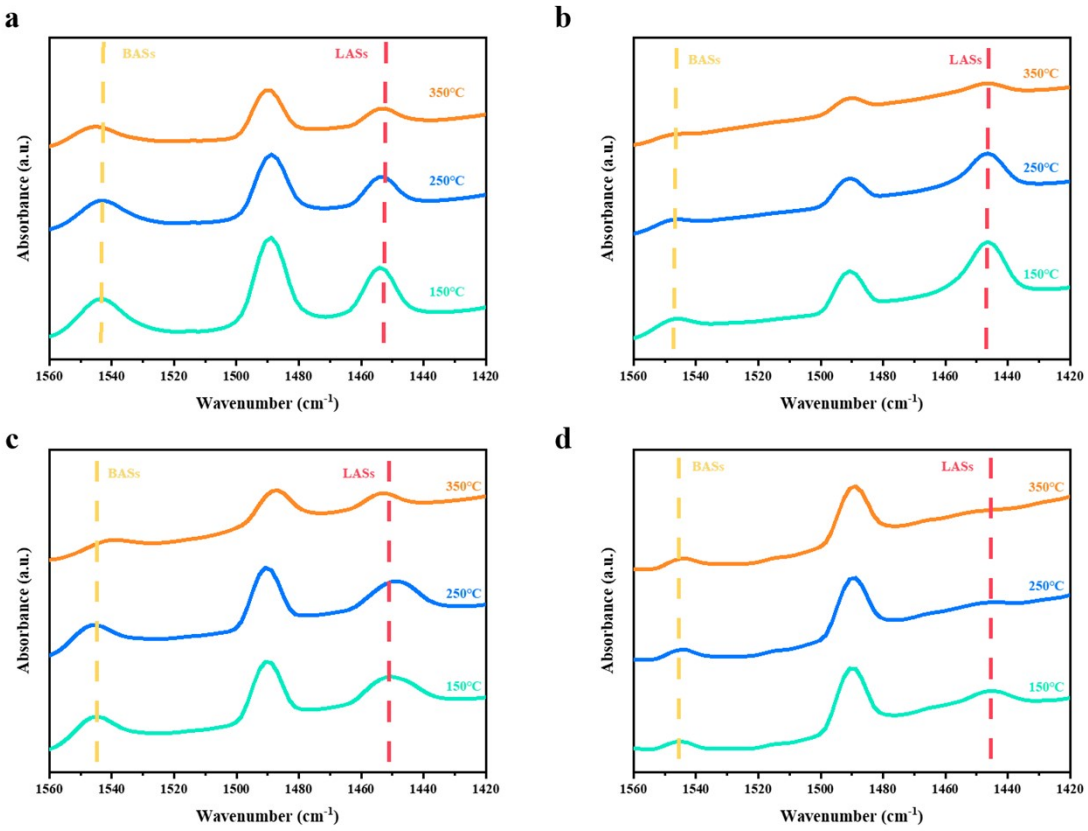

235

236 Fig.S11 Py-FTIR spectra of (a) Beta-C, (b) SPP, (c) ZSM-5, (d) ZSM-5-M at 150 ℃,

237 250 ℃, 350 ℃ respectively

238

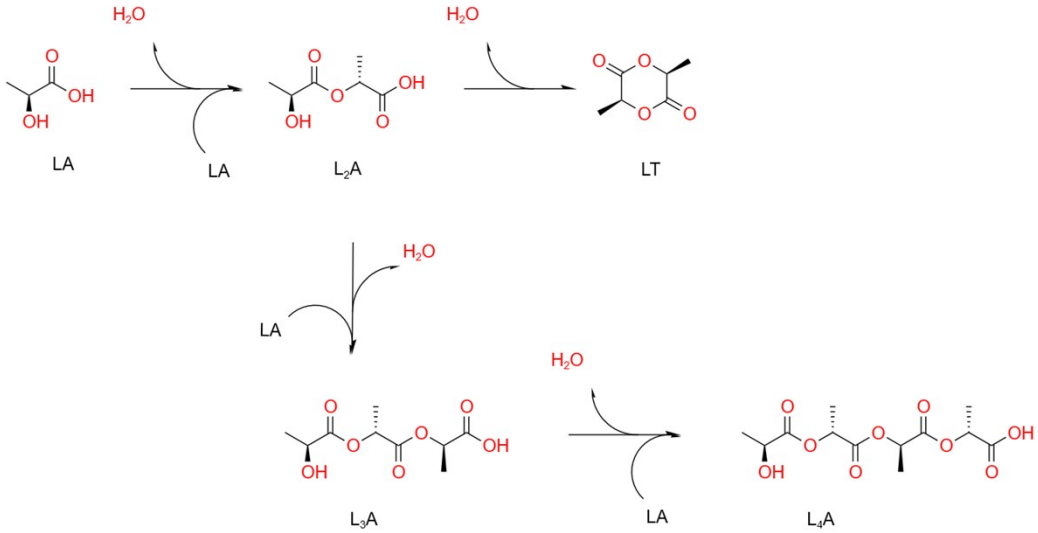

239

240

241 Fig.S12 Reaction pathways from LA to LT

242

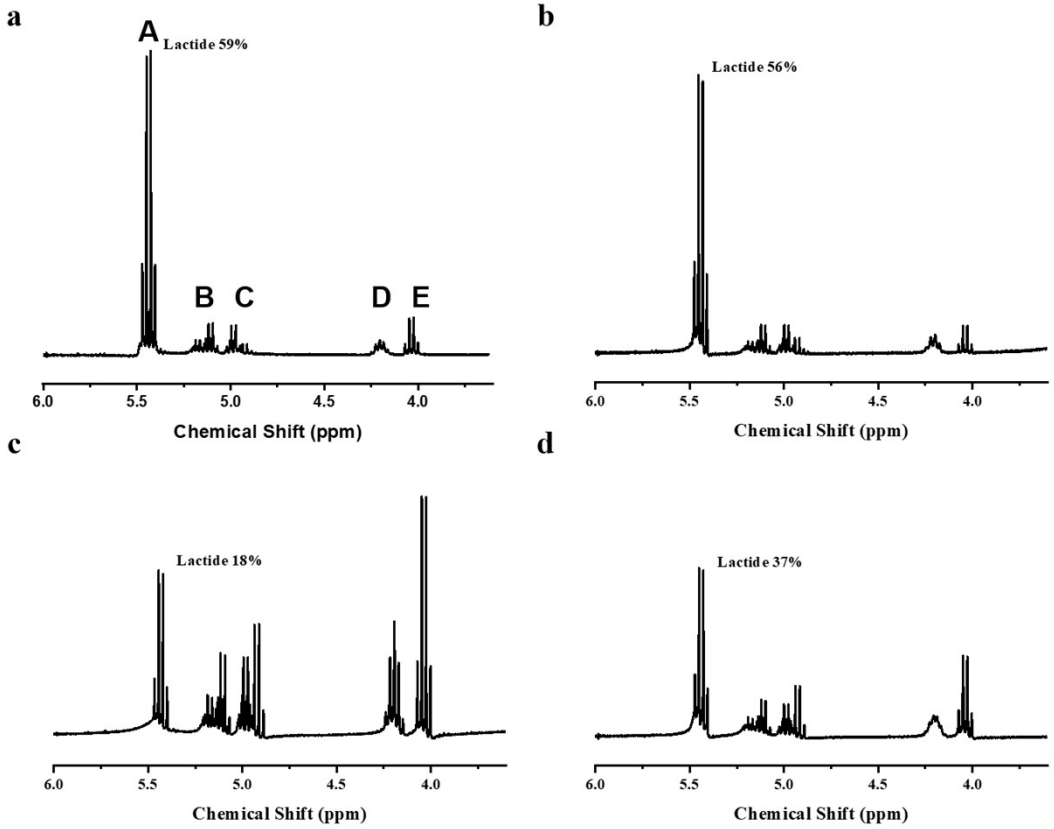

243

244 Fig.S13 Typical ^{1}H-NMR analysis (in DMSO-d_6) of the reaction mixture after 5 hours

245 over (a) Beta-C, (b) SPP, (c) ZSM-5, (d) ZSM-5-M

246

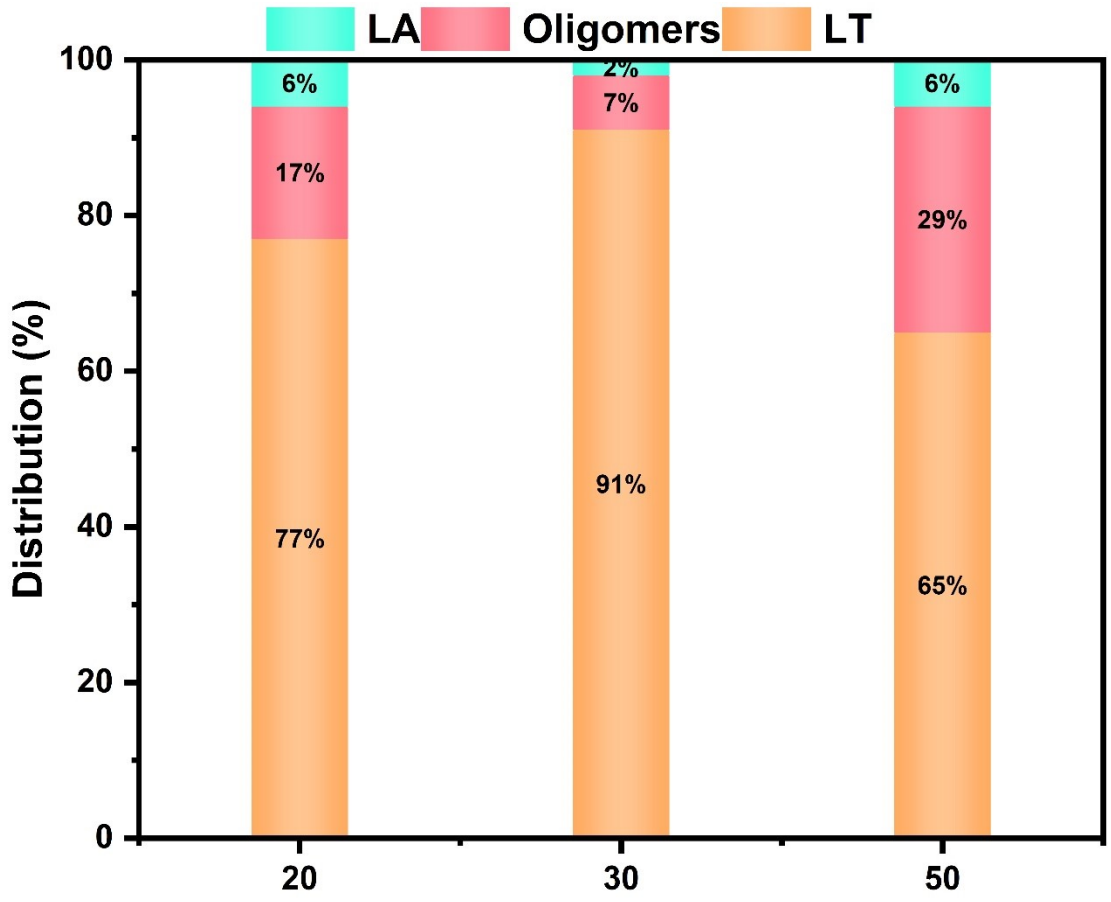

Fig.S14 Influence of SAR of EMM-17 on the reaction in toluene.

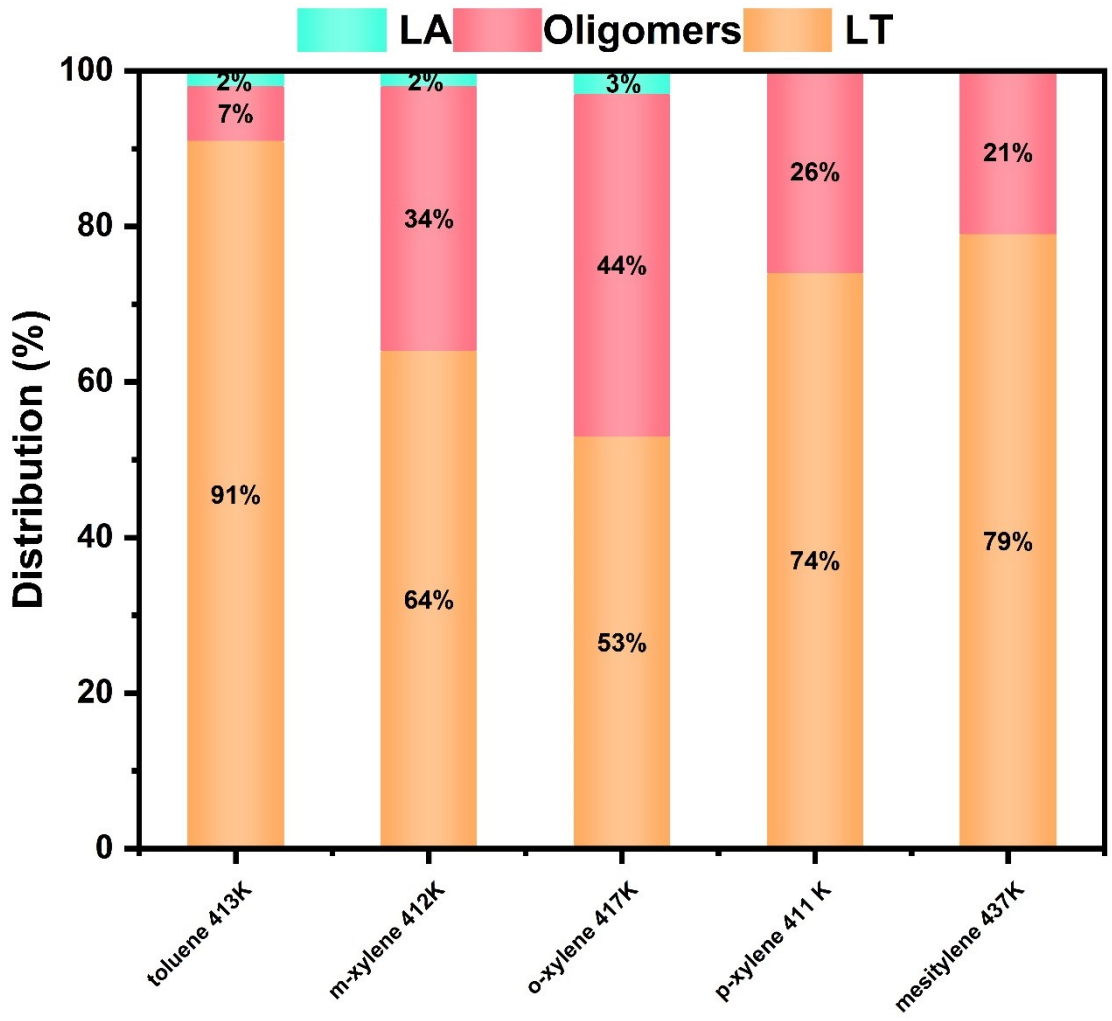

Fig.S15 Influence of different solvents. The boiling point (T_b) of each solvent is indicated in the figure. The heating input of the oil bath was set at T_b.

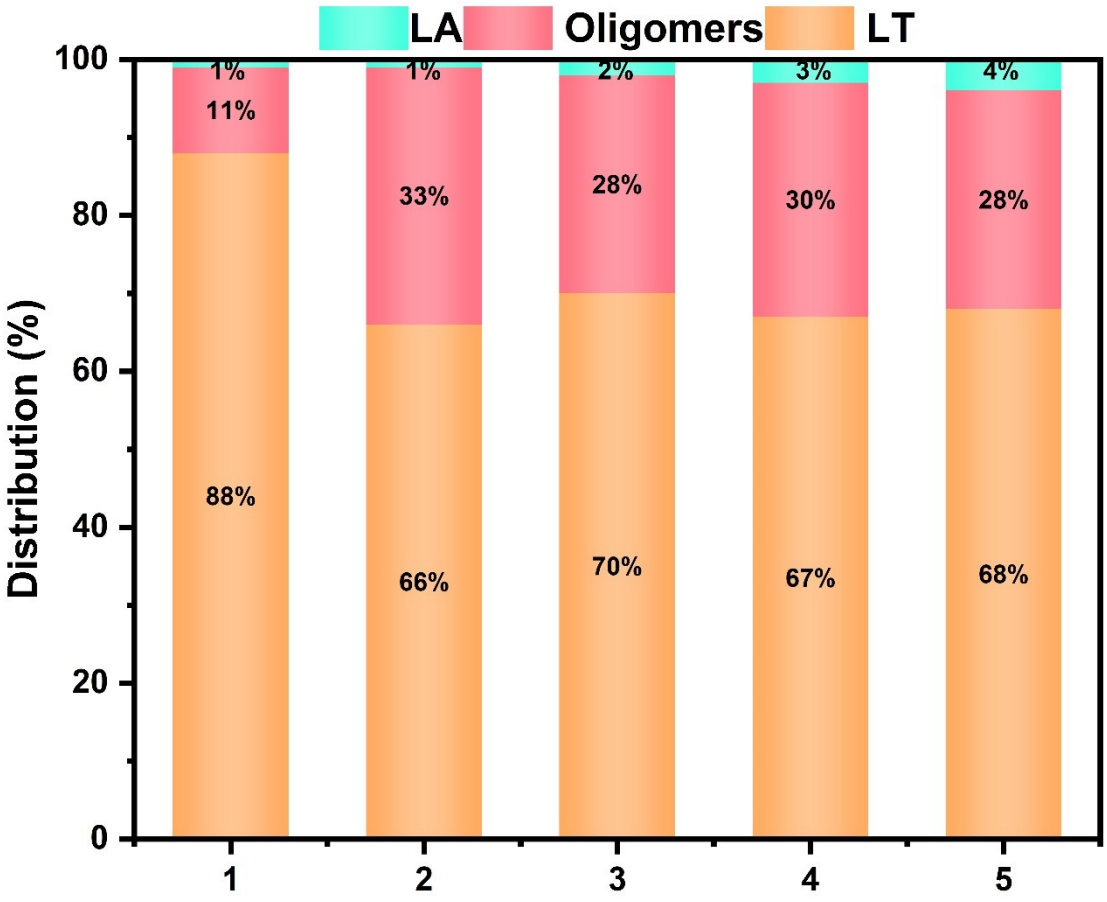

Fig.S16 Recyclable tests of EMM-17.

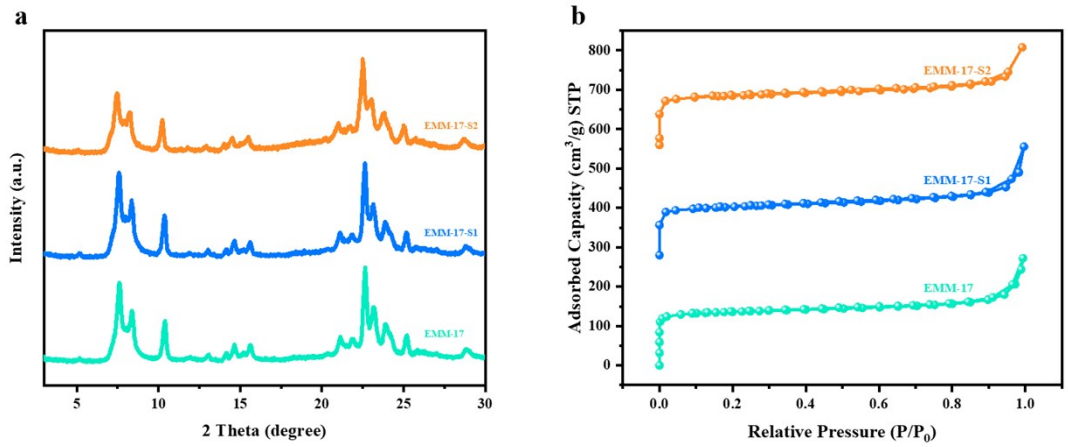

Fig.S17 (a) PXRD patterns and (b) N_2 adsorption-desorption isotherms of EMM-17, EMM-17-S1 and EMM-17-S2

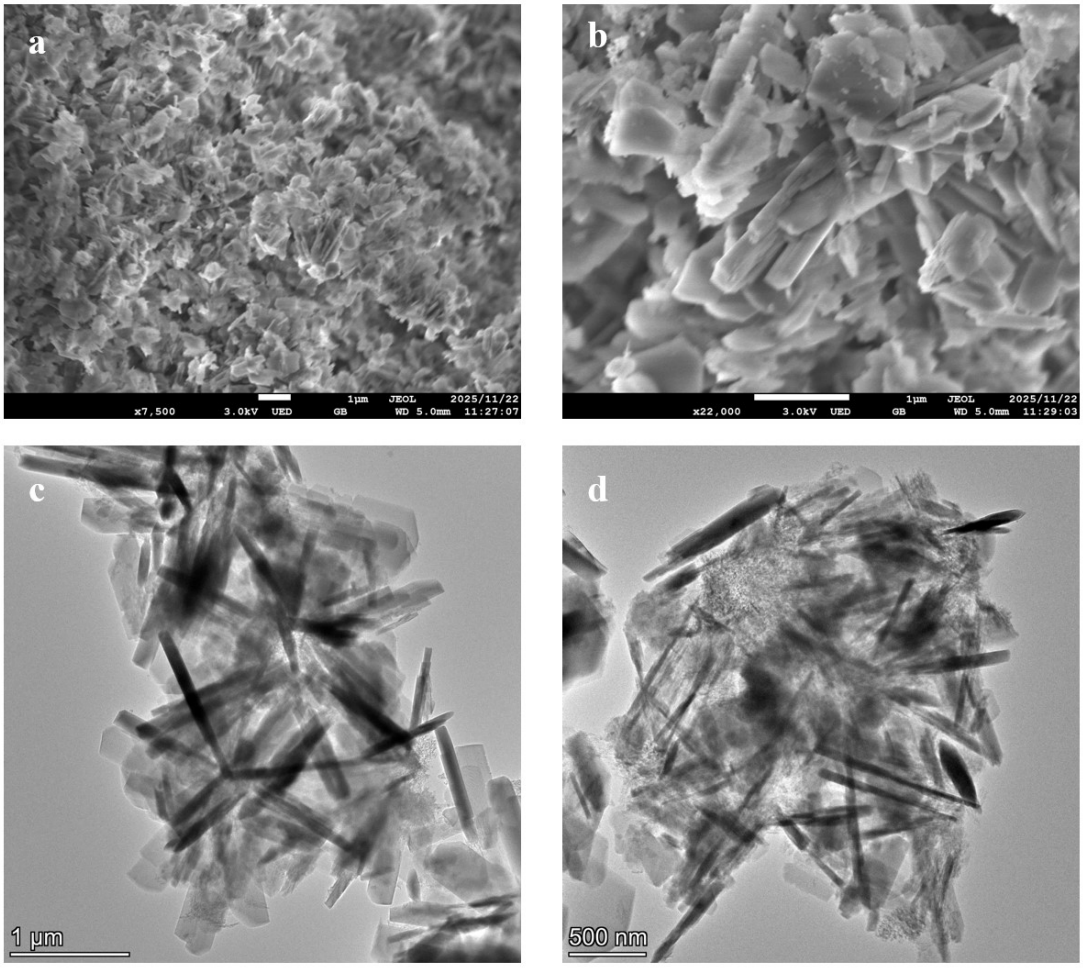

Fig.S18 (a, b) SEM images and (c, d) TEM images of EMM-17-S1

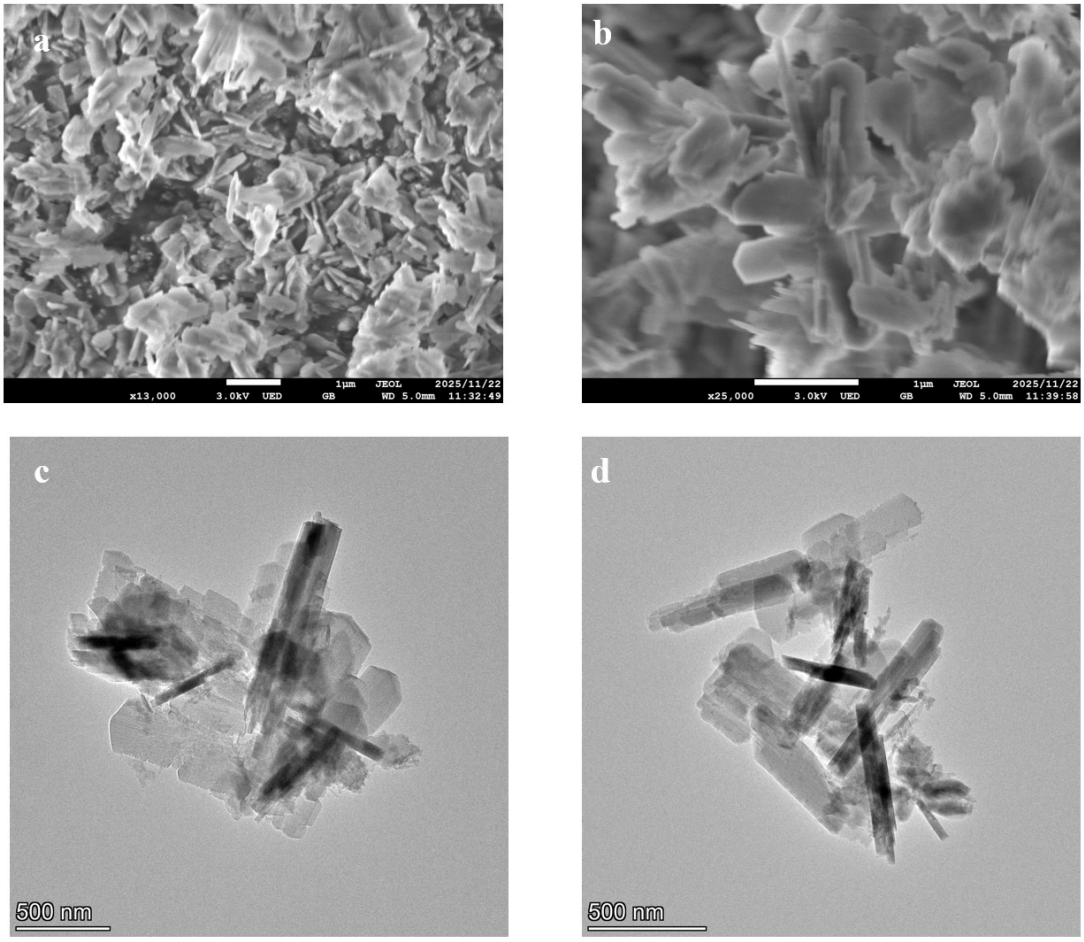

Fig.S19 (a, b) SEM images and (c, d) TEM images of EMM-17-S2

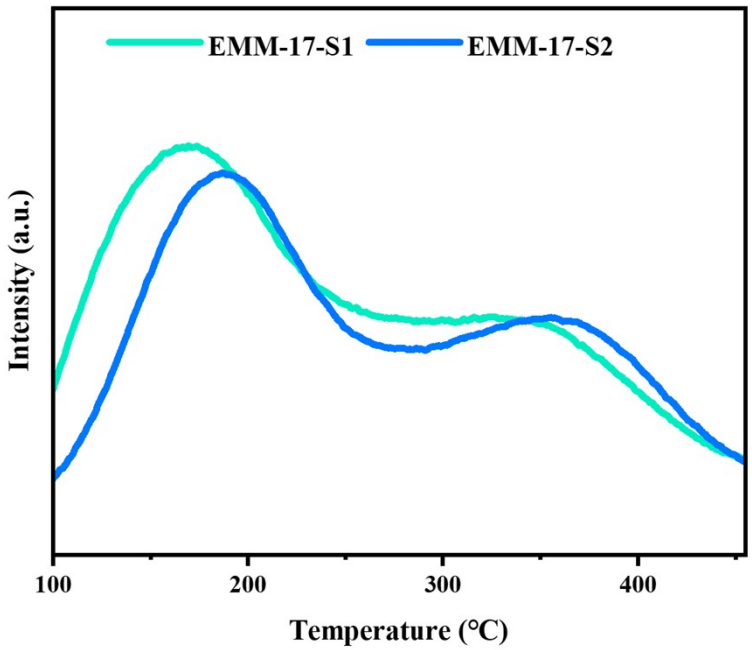

267

268 Fig.S20 NH_3-TPD profiles of EMM-17-S1 and EMM-17-S2

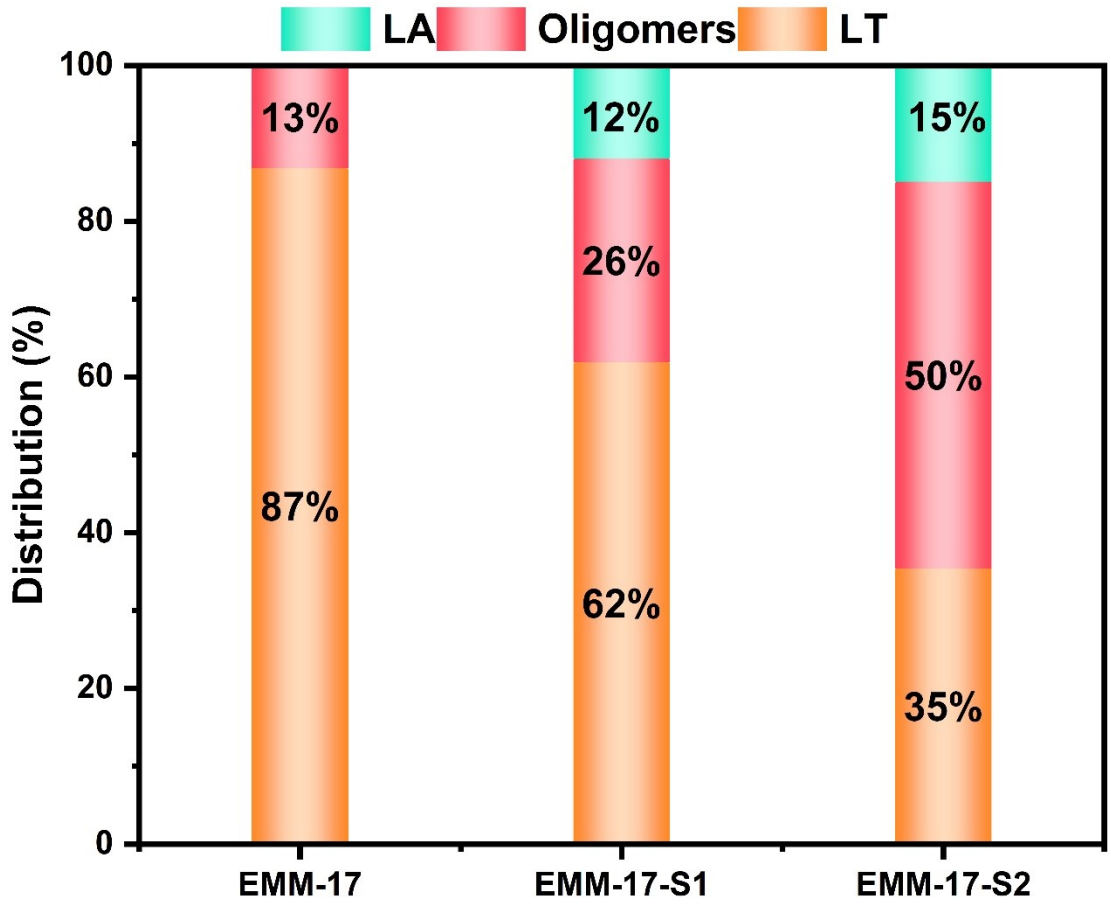

Fig.S21 Product distribution of EMM-17, EMM-17-S1 and EMM-17-S2. Distribution was determined by HPLC.

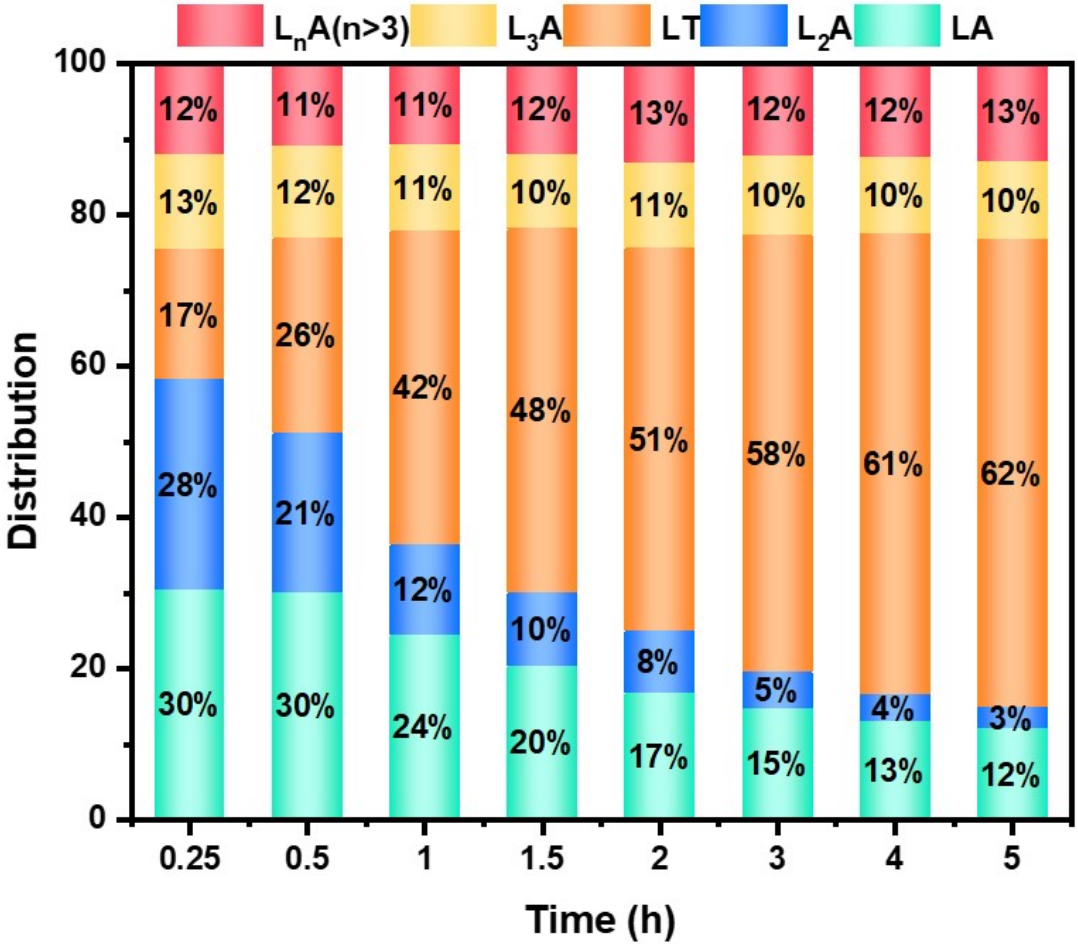

Fig.S22 HPLC profiles of LA conversion over EMM-17-S1

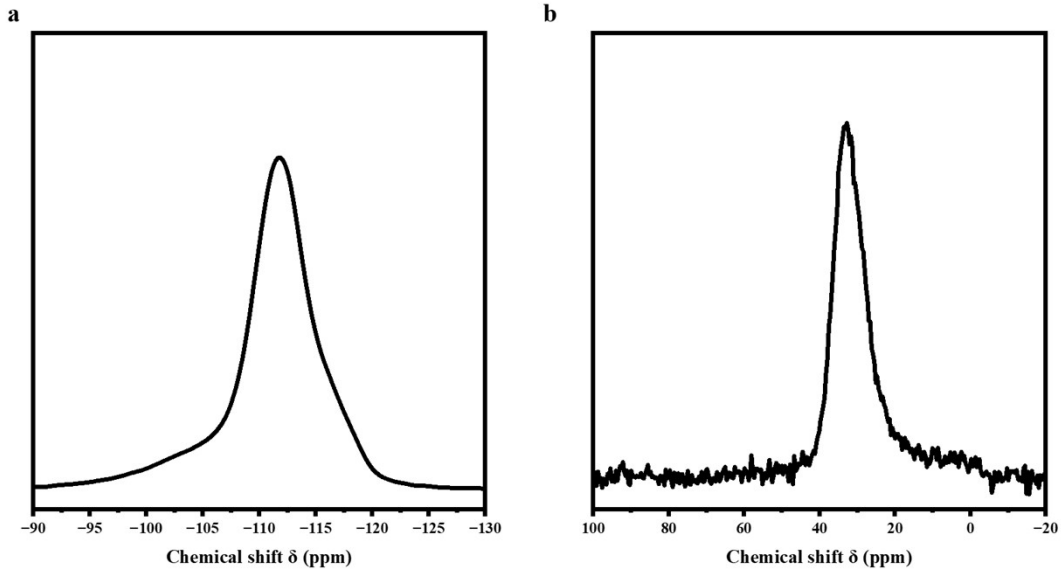

276

277 Fig.S23 (a) ^{29}Si MAS NMR and (b) ^{27}Al MAS NMR spectra of EMM-17-S2

278

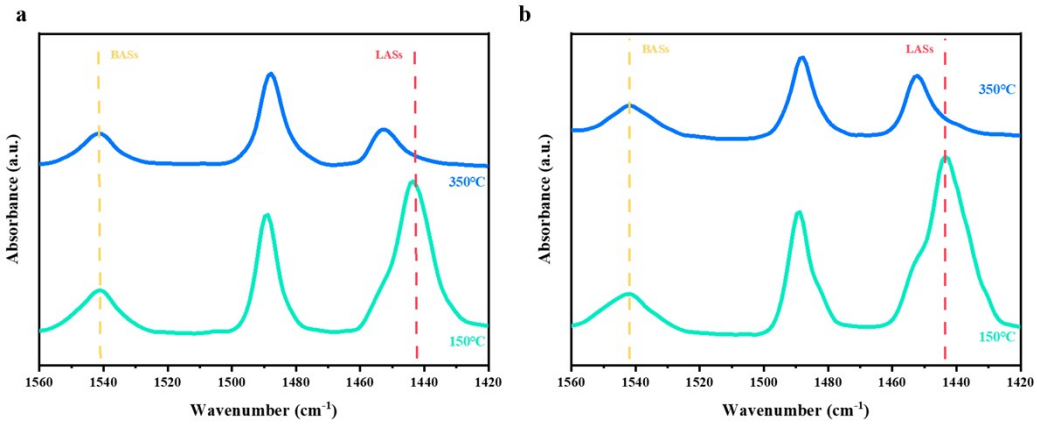

279

280 Fig.S24 Py-FTIR spectra of (a)EMM-17 and (b)EMM-17-S2 at 150 ℃, 350 ℃

281 respectively

282

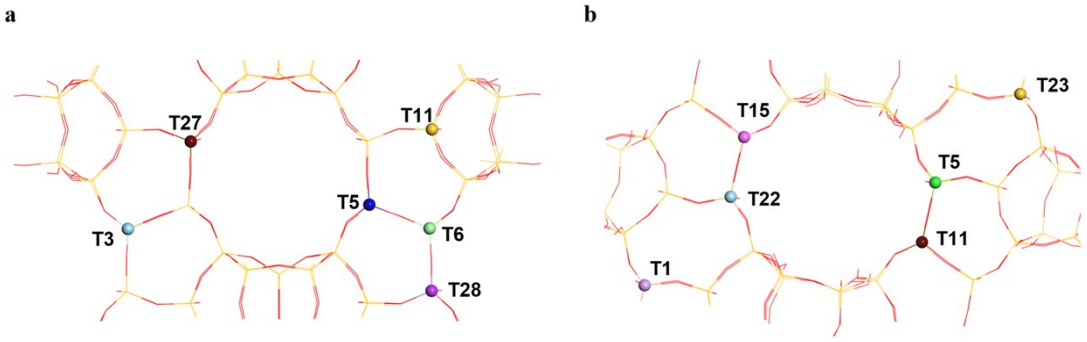

283

284 Fig.S25 6 unequal T-sites of (a)EMM-17A and (b) EMM-17B

285

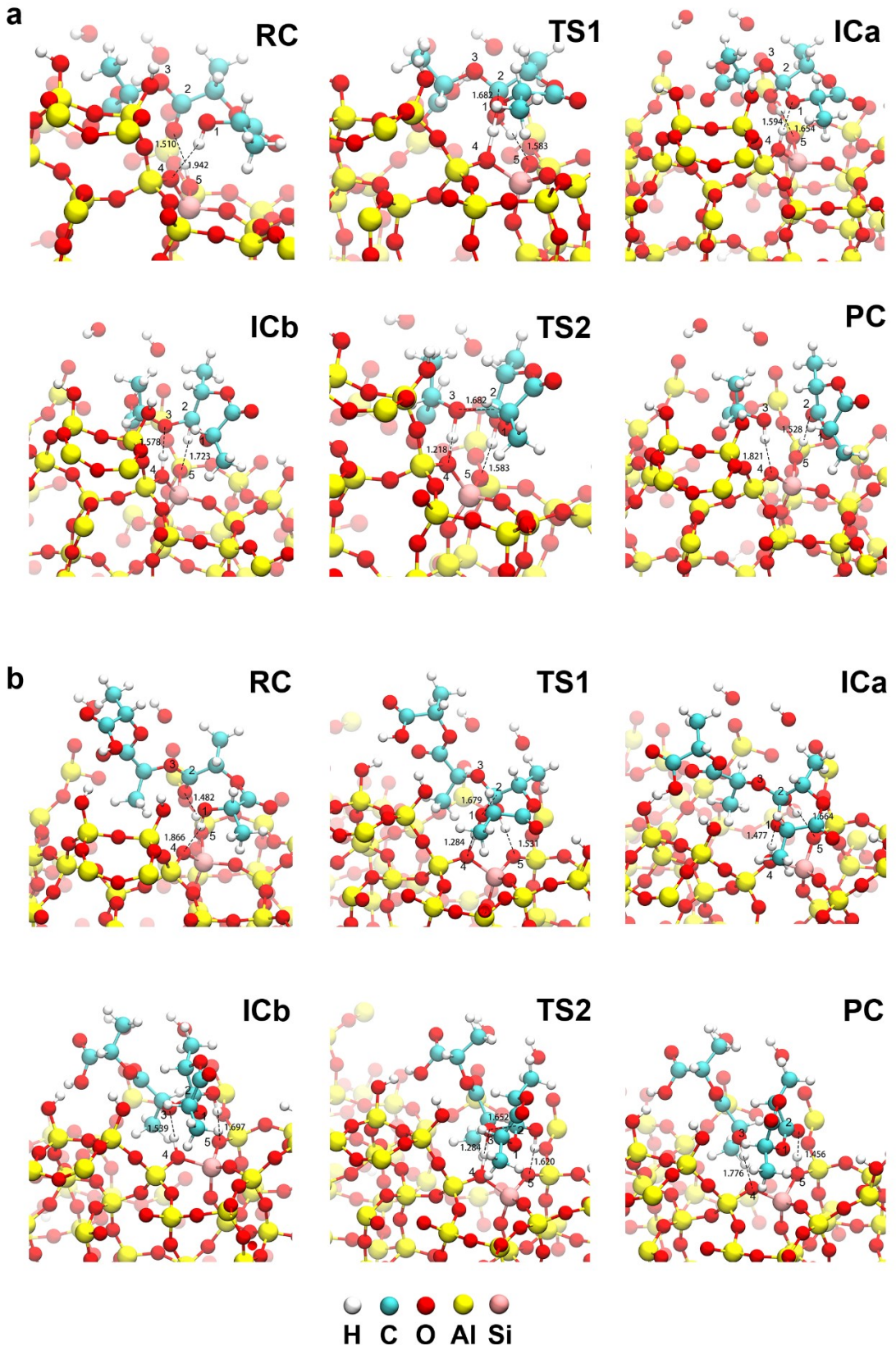

Fig.S26 PBE/PAW optimized structure of species involved in the LT formation from (a) L_3A and (b) L_4A over EMM-17A

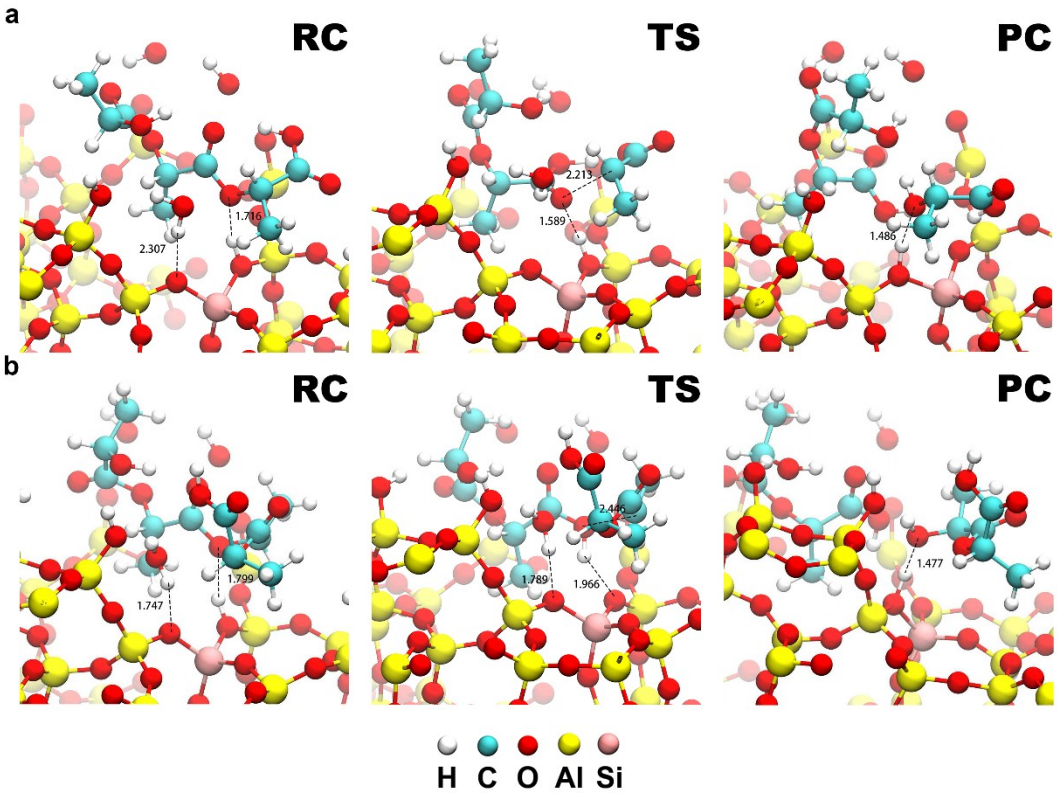

289

290 Fig.S27 PBE/PAW optimized structure of species involved in the L_2A formation from

291 (a) L_3A and (b) L_4A over EMM-17A

292

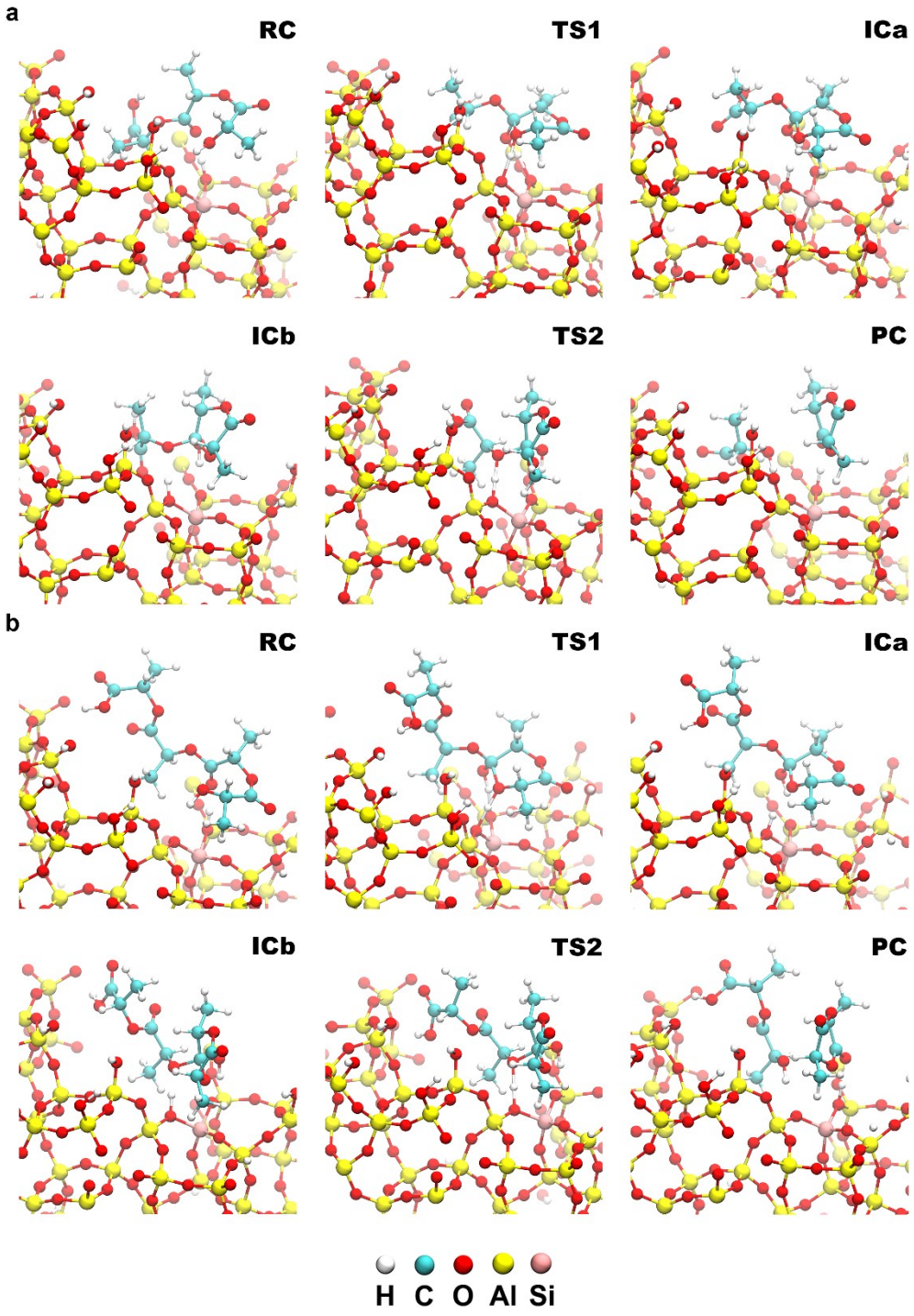

Fig.S28 PBE/PAW optimized structure of species involved in the LT formation from (a) L_3A and (b) L_4A over EMM-17B

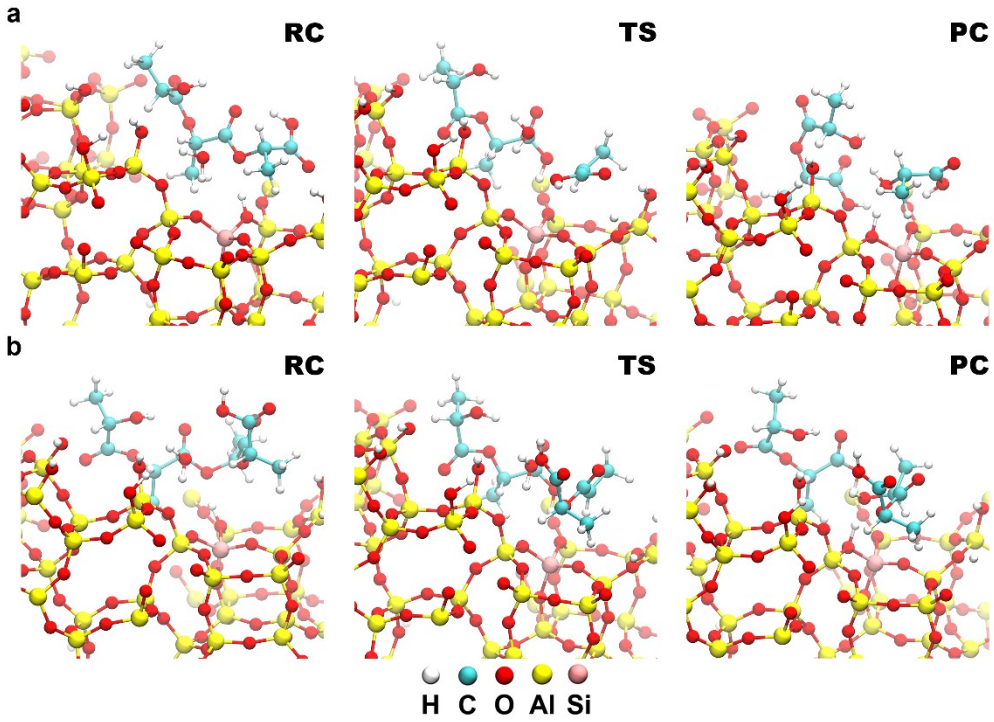

Fig.S29 PBE/PAW optimized structure of species involved in the L_2A formation from (a) L_3A and (b) L_4A over EMM-17B

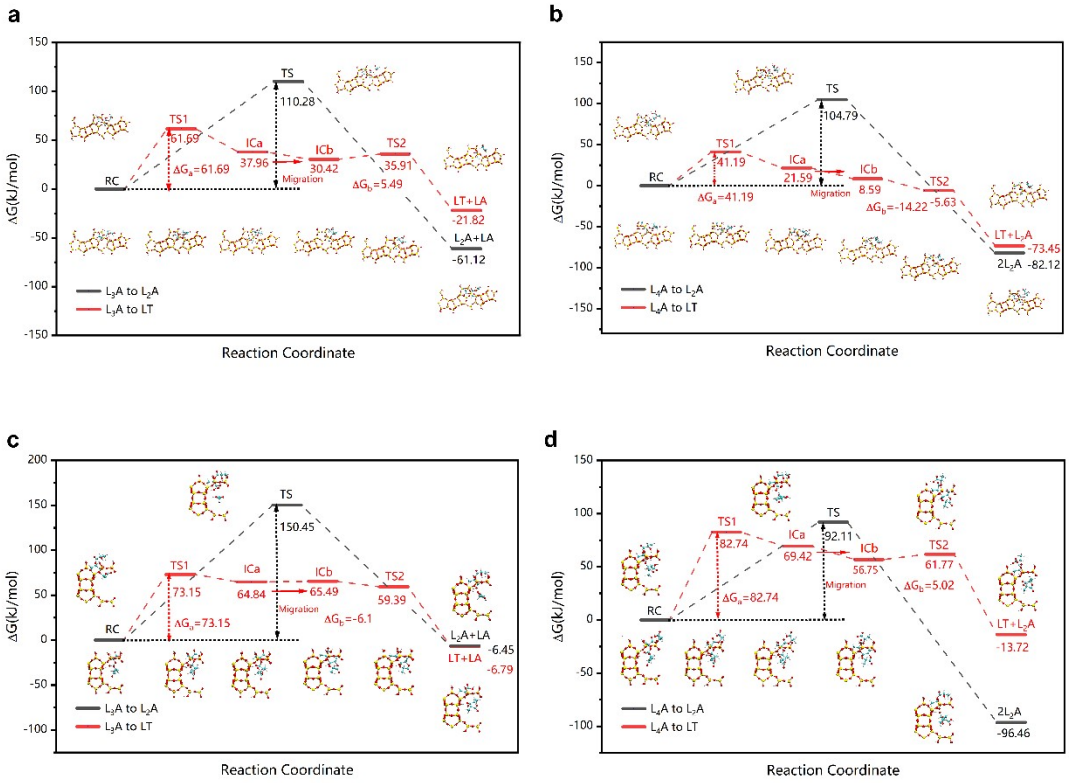

Fig.S30 Free energy profiles of the conversion of L_3A and L_4A to LT or L_2A on the external surface of (a, b) Beta [101] and (c, d) Beta [001]

306 Table S1 Textural properties of various samples by N_2 sorption

Samples	S_{BET}[a](m^2g^{-1})	S_{micro}[b](m^2g^{-1})	S_{ext}[b](m^2g^{-1})	V_{total}[c](cm^3g^{-1})	V_{micro}[b](cm^3g^{-1})	V_{meso}[d](cm^3g^{-1})
EMM-17	**566**	**428**	**138**	**0.57**	**0.18**	**0.39**
Beta	**646**	**588**	**58**	**0.49**	**0.23**	**0.26**
SPP	**753**	**484**	**269**	**1.08**	**0.22**	**0.86**
ZSM-5	**437**	**385**	**52**	**0.26**	**0.17**	**0.09**
ZSM-5-M	**399**	**271**	**128**	**0.28**	**0.11**	**0.17**

307 [a] S_{BET}: Total surface area, calculated by the BET method.

308 [b] S_{micro}: micropore surface area, S_{ext}: external surface area, and V_{micro}: micropore

309 volume, calculated by the t-plot method.

310 [c] Total pore volume of N_2 adsorbed at P/P_0=0.99.

311 [d] V_{meso}: mesopore volume, $V_{meso} = V_{total} - V_{micro}$.

312

313 Table S2 Textural properties of EMM-17, EMM-17-S1 and EMM-17-S2 by N_2

314 sorption

Samples	S_{BET}[a](m^2g^{-1})	S_{micro}[b](m^2g^{-1})	S_{ext}[b](m^2g^{-1})	V_{total}[c](cm^3g^{-1})	V_{micro}[b](cm^3g^{-1})	V_{meso}[d](cm^3g^{-1})
EMM-17	**532**	**474**	**58**	**0.39**	**0.19**	**0.20**
EMM-17-S1	**466**	**394**	**72**	**0.38**	**0.16**	**0.22**
EMM-17-S2	**487**	**406**	**81**	**0.38**	**0.16**	**0.22**

315

316

317 Table S3 Adsorption energy on different T sites of EMM-17A

EMM-17A Al site	$L_3A \rightarrow LT$ Eads (kJ/mol)	$L_4A \rightarrow LT$ Eads (kJ/mol)
T3	**-206.43**	**-207.74**
T5	**-211.54**	**-216.69**
T6	**-153.97**	**-200.71**
T11	**-166.36**	**-138.37**
T27	**-183.01**	**-190.21**
T28	**-183.89**	**-157.15**

318

319

320 Table S4 Adsorption energy on different T sites of EMM-17B

EMM-17B Al site	$L_3A \rightarrow LT$ Eads (kJ/mol)	$L_4A \rightarrow LT$ Eads (kJ/mol)
T1	**-143.18**	**-141.25**
T5	**-170.04**	**-170.67**
T11	**-185.39**	**-188.32**
T15	**-171.59**	**-261.50**
T22	**-150.58**	**-230.08**
T23	**-145.23**	**-101.55**

321

322

Table S5 Free energy of L_3A and L_4A hydrolysis and LT production on the external surface of EMM-17 and Beta

kJ/mol	EMM-17A		EMM-17B		Beta [101]		Beta [001]	
	TS1	TS2	TS1	TS2	TS1	TS2	TS1	TS2
$L_3A \rightarrow L_2A$	76.69		159.29		110.28		150.45	
$L_4A \rightarrow L_2A$	117.64		102.44		104.79		92.11	
$L_3A \rightarrow LT$	36.79	14.73	33.96	20.07	61.69	5.49	73.15	-6.1
$L_4A \rightarrow LT$	31.98	1.51	94.52	31.28	41.19	-14.22	82.74	5.02

References

1. T. W. Beutel, A. M. Willard, C. Lee, M. S. Martinez and R. Dugan, *J. Phys. Chem. C*, 2021, **125**, 8518-8532.
2. H. K. Heinichen and W. F. Hölderich, *J. Catal.*, 1999, **185**, 408-414.
3. G. Kresse and J. Furthmüller, *Comput. Mater. Sci.*, 1996, **6**, 15-50.
4. P. E. Blöchl, *Phys. Rev. B*, 1994, **50**, 17953-17979.
5. G. Kresse and D. Joubert, *Phys. Rev. B*, 1999, **59**, 1758-1775.
6. J. P. Perdew, K. Burke and M. Ernzerhof, *Phys. Rev. Lett.*, 1996, **77**, 3865-3868.
7. G. Henkelman, B. P. Uberuaga and H. Jónsson, *J. Chem. Phys.*, 2000, **113**, 9901-9904.
8. G. Henkelman and H. Jónsson, *J. Chem. Phys.* 1999, **111**, 7010-7022.
9. M. Dusselier, P. Van Wouwe, A. Dewaele, P. A. Jacobs and B. F. Sels, *Science*, 2015, **349**, 78-80.